Author's Accepted Manuscript

The use of video imagery to analyse groundwater and shoreline dynamics on a dissipative beach

Christien E. Huisman, Karin R. Bryan, Giovanni Coco, B.G. Ruessink

www.elsevier.com/locate/csr

Cite this article as: Christien E. Huisman, Karin R. Bryan, Giovanni Coco and B.G. Ruessink, The use of video imagery to analyse groundwater and shoreline dynamics on a dissipative beach, *Continental Shelf Research*, doi:10.1016/j.csr.2011.07.013

The use of video imagery to analyse groundwater and shoreline dynamics on a dissipative beach

Christien E. Huisman[1], Karin R. Bryan[2], Giovanni Coco[3,4] and B.G. Ruessink[1]

[1] Department of Physical Geography, Faculty of Geosciences, Institute for Marine and Atmospheric Research, Utrecht University, The Netherlands
[2] Department of Earth and Ocean Sciences, University of Waikato, Hamilton, New Zealand
[3] National Institute of Water and Atmospheric Research, Hamilton, New Zealand
[4] Now at Environmental Hydraulics Institute, "IH Cantabria", Universidad de Cantabria, Santander, Spain

Corresponding Author: Mrs. Christien E. Huisman, MSc.

Abstract

Groundwater seepage is known to influence beach erosion and accretion processes. However, field measurements of the variation of the groundwater seepage line (GWSL) and the vertical elevation difference between the GWSL and the shoreline are limited. We developed a methodology to extract the temporal variability of the shoreline and the wet-dry boundary using video imagery, with the overarching aim to examine elevation differences between the wet-dry boundary and the shoreline position in relation to rainfall and wave characteristics, during a tidal cycle. The wet-dry boundary was detected from 10-minute time-averaged images collected at Ngaranui Beach, Raglan, New Zealand. An algorithm discriminated between the dry and wet cells using a threshold related to the maximum of the red, green and blue intensities in Hue-Saturation-Value. Field measurements showed this corresponded to the location where the watertable was within 2 cm of the beachface surface. Timestacks, time series of pixels extracted from cross-shore transects in the video imagery, were used to determine the location of the shoreline by manually digitizing the maximum run-up and minimum run-down location for each swash cycle, and averaging the result. In our test data set of 14 days covering a range of wave and rainfall conditions, we found 6 days when the elevation difference between the wet-dry boundary and the shoreline remained approximately constant during the tidal cycle. For these days, the wet-dry boundary corresponded to the upper limit of the swash zone. On the other 8 days, the wet-dry boundary and the shoreline decoupled with falling tide, leading to elevation differences of up to 2.5 m at low tide. Elevation differences between the GWSL and the shoreline at low-tide were particularly large when the cumulative rainfall in the preceding month was greater than 200 mm. This research shows that the wet-dry boundary (such as often used in video shoreline-finding algorithms) is related to groundwater seepage on low-sloped, medium to fine sand beaches such as Ngaranui

Beach (mean grain size ~ 0.27 mm, beach slope ~1:70) and may not be a good indicator of the

position of the shoreline.

1 Introduction

The dynamics of the beach groundwater table in the swash zone are of interest to researchers in the field of geomorphology, coastal engineering, sedimentology and groundwater hydrology (e.g. Baird and Horn, 1996; Horn, 2002; Horn, 2006; Nielsen, 1990; Turner, 1993). The elevation of the beach water table alters erosion and accretion processes in the swash zone (e.g. Butt et al., 2001; Eliot and Clarke, 1988; Grant, 1948; Turner, 1993; Coco et al., 2004). When a high water table causes the beach face to be saturated, erosion is favoured because sediment movement is promoted by outflow of water from the water table and sediment dilation (e.g. Eliot and Clarke, 1988; Grant, 1948; Horn, 2002; Turner, 1993; Turner, 1995). In some cases, artificial lowering of the beach water table, e.g. beach dewatering, is carried out to stimulate sedimentation. These beach protection measures have had limited success probably because our understanding of the processes controlling the influence of beach groundwater on beach erosion is still limited (Baird and Horn, 1996; Horn, 2002; Turner and Leatherman, 1997).

Wave run-up, tidal variation and rainfall may cause the elevation of the beach water table to be above the elevation of the mean sea surface (Turner et al., 1997). Water flows into the beach face if the sea surface is higher than the level of the groundwater table and vice versa. This process can occur on a number of different time scales. If the mean sea level (including set-up and storm-related changes) is higher than the mean water table there will be a mean flow landward; if it is lower the mean flow will be seaward. Superimposed on this mean pattern are the tidal variations, where landward flows occur at high tide and seaward flows at low tide, and individual swash patterns where swash crests cause landward flows. The rate of flow depends on the hydraulic conductivity and the horizontal pressure gradient. If the seaward pressure gradient is high and/or the hydraulic conductivity of the beach sediments is

low, then a falling water level (such as is caused by the tide) can cause a seepage face on the beach face, below the point where the beach watertable intersects the beach face and the groundwater exfiltrates (Raubenheimer et al., 1999; Turner, 1993). The groundwater seepage line (GWSL) forms at the interface between the unsaturated and saturated beachface (Horn, 2002; Horn, 2006). It can be identified by its shiny appearance due to water that 'sheets' on top of the beach (Cartwright et al., 2006; Horn, 2002), and is most likely to form on fine-grained, low-sloping beaches with large tidal ranges (Jackson et al., 1999; Turner et al., 1997).

The movement of the GWSL and the (de-)coupling of this wet-dry boundary from the tide have been extensively modelled (Baird et al., 1998; Cartwright et al., 2006; Li and Barry, 2000; Li et al., 2002; Li et al., 2000; Turner, 1993; Turner, 1995). However, as pointed out by Baird and Horn (1996), improvements in field monitoring and modelling beach groundwater dynamics are needed to incorporate the influence of groundwater dynamics on swash sediment dynamics. For example, simple models include only tidal variation and sediment characteristics, and not the variation of the inland water table in their formulation (Turner, 1995). Yet, presumably large precipitation events that elevate the water table will favour conditions for decoupling. Baird et al. (1998), Cartwright et al. (2006), Li and Barry (2000), Li et al. (2002), Li et al. (2000), Turner (1993) and Turner (1995) specifically suggest the use of video imagery to monitor groundwater seepage to provide better insight in the width of the seepage face and swash dynamics. Over the last decade, video-based remote sensing techniques are increasingly-used to study beach evolution, because they provide continuous and automated data collection (Aarninkhof et al., 2003; Madsen and Plant, 2001; Plant et al., 2007; Plant and Holman, 1997). However, their application to measuring groundwater seepage has not been pursued yet.

The objective of this paper is two-fold. Firstly, we present and test a video-based method to extract wet-dry boundary and shoreline locations simultaneously, with a high spatial (cross-shore) and temporal resolution from video images collected at Ngaranui Beach, New Zealand (Section 2). This method is different from previous methods in that it does not assume that the shoreline and wet-dry boundary are at the same location. Secondly, we use this technique to extract GWSL observations from video over a range of conditions to determine to what degree the GWSL variation follows the shoreline and to what degree it depends on other factors such as the wave conditions and cumulative rainfall (Section 3). This demonstrates under what conditions our method is relevant. In Section 4 and 5, we discuss and summarize our main findings.

2 Site description

Ngaranui beach, located near Raglan on the North Island of New Zealand, is a dissipative beach of approximately 1800 m length and faces northwest toward the Tasman Sea (Figure 1). The beach is constrained by a steep (~1:5) dune ridge and by headlands at the south and east side. At the north side, the beach curves into Raglan Estuary, a drowned ancient river valley (Morris et al., 2007). The beach contains black volcanic sediments with a median grain size of 0.31 mm (Laurent, 2000). The beach slope is roughly 0.8 degrees (~1:70). Monthly surveys along four cross-shore transects performed in 2009 by Wood (2009) showed limited spatial or temporal variation, with beach volumes changing by $\sim \pm 10\%$ between winter and summer. The tidal range is between 2−3 m (spring tide) and 1.5−1.8 m (neap tide) (Walters et al., 2001). Wave hindcasts (Gorman et al., 2003), for a position at intermediate depth off-shore from Ngaranui beach (depth=11 m, position: LAT −37.813553; LON 174.802104), show the annual mean significant wave height to be 1.8 m and the mean wave period 8 s. The

6

mean daily precipitation, based on daily observations in Raglan Harbour

(http://cliflo.niwa.co.nz/), is 3 mm. Most rain falls in the southern hemisphere winter, between

June and October. Rainfall in excess of 90 mm per day sometimes occurs in autumn and

spring. After a day of intense rain, water drains from the headlands onto the beach (Figure 2).

3 Methods

3.1 Data acquisition

Ngaranui Beach has been monitored since August 2007 by a Cam-Era video system (e.g.

Almar et al., 2008; Gallop et al., 2011). The video unit comprises a Lumenera LE 375 7.7-mm

color CCD video camera with a 25.5-mm fixed-focal-length lens. The video camera is

situated on the headland south of the beach at 94 m above mean sea level. The video system

covers an area of 1.5 km alongshore and 150-800 m cross-shore, with the pixel footprint

ranging from 0.11 m × 0.56 m at the south end of the beach and 0.59 m × 5.96 m at the

northern end which was further away from the camera. Every half hour during daylight

conditions, an on-site computer collects a snapshot image, three timestack images and an

averaged image. Averages and timestacks were collected over 10 minutes of video footage

collected at 2 Hz, and timestacks are time series of pixels collected along a cross-shore

transect from each frame (e.g. Aagaard and Holm, 1989; Salmon et al., 2007; Stockdon et al.,

2006). Here, we focus on data gathered from the timestacks and the time-averaged images.

The timestacks stack locations are 1300 m (timestack 1), 800 m (timestack 2), 600 m

(timestack 3) from the camera. The cross-shore resolution of the time-stacks ranged from 0.3-

0.4 m at timestack 1 to 0.07-0.15 m at timestack 3. Each timestack covered part of the sea and

the beach and thus contains the motion of the incident waves as they run up and down the

beach as swash and backwash. An example timestack with run-up oscillations is provided in

Figure 3. The alongshore resolution of the time-averaged images is approximately 3 m at

1300 m (timestack 1) from the camera, decreasing to 0.2 m in the vicinity of timestack 3. An example time-averaged image is provided in Figure 4A.

We define the shoreline as the average of the swash timeseries, which is consistent with the definition of mean shoreline (including setup) used in other video studies (e.g Holland and Holman 1993; Stockdon et al., 2006). Note that this could be different than the definition of shoreline as the location where the mean water surface intersects the beach face (such as might be measured with an array of stilling wells). Bryan et al. (2008) demonstrated the existence of a slight horizontal difference of order 1.5 m on an intermediate, medium sand beach. Since automated detection of the shoreline on this black sand beach defied existing methodologies (e.g. Aarninkhof et al., 2003; Boak and Turner, 2005), run-up minima (lower backwash limit) and maxima (upper up-rush limit) were digitized manually from each timestack (Figure 3), after Aagaard and Holm (1989). The lower backwash limit was identified as the intersection of the backwash and the uprush of the next wave. The shoreline position was defined as the mean of all maxima and minima. Figure 4A (white circles) shows an example of the detected shoreline positions along the cross-shore timestacks.

To extract the wet-dry boundary, the Red-Green-Blue (RGB) time-averaged images were transformed into Hue-Saturation-Value-space (HSV-space) using the Matlab® 'rgb2hsv' function. Although there are a number of different models for calculating the Saturation from RGB values (Russ, 2006), the Matlab® algorithm simply calculates the Value (V) as the maximum of the red, green and blue intensities at each pixel (following the method of Smith, 1978). HSV-space corresponds more to human perception than RGB-space, and treats colour (hue, saturation) and luminance (brightness or value) information separately (Russ, 2006). The wet-dry boundary was detected using a thresholding algorithm that discriminates between

8

the dry and wet beach based on the Value (V), because V was found to be the only measure that consistently detected the wet-dry boundary in all tested weather conditions (see validation section below). For each of the selected time-averaged images, the algorithm requires a subjective definition of an alongshore line over the dry beach, and an alongshore line over the sea. These lines limit the region over which the processing software searches, thus limiting irregularities in the Value caused by the areas that rarely get inundated (e.g. dune grasses, and upper beach driftwood). In between these lines, the algorithm extracts the Value (V) from each row in the oblique image, and smoothes the resulting V using a moving-average smoothing algorithm with a grid size of 10 pixels (Figure 4B). Given an approximate cross-shore resolution of 0.11 m at time stack 3 and 0.35 m at timestack 1, this averaging smoothes features in the image of 1 - 3.5 m size, roughly corresponding to removing the effect of people sitting on the beach, or large pieces of driftwood. In test cases of 10 randomly-chosen images, changing this averaging range from 5 to 15 pixels changed the detection of the seepage line by <3 pixels.The seepage-line detection algorithms then finds the pixel where the Value (V) is smaller than a threshold value, here taken as the V composed of the 25% of V at the dry beach and 75% of V at the sea. Figure 4B provides an example for a single row of pixels from the image, and the entire alongshore line of the detected wet-dry boundary (Figure 4A).

Information extracted from the images was rectified to real world coordinates. Rectification was done after detection (rather than rectifying the whole image and using this for detection) because rectifying the whole image was computationally intensive, added inaccuracy due to interpolation methods used and finally does not easily allow the image to be rectified to multiple vertical levels (the shoreline and seepage line are generally at different levels). Rectifying pixel coordinates of the seepage line allows different vertical levels to be used for

9

different areas of the image. The 2D pixel coordinates were corrected for distortions related to the camera lens using the standard photogrammetric techniques outlined by Heikkilä and Silven (1997). The corrected 2D oblique pixel coordinates (u,v) were converted to ground coordinates (x,y,z) using the colinearity equations and a known elevation. For the rectification of shoreline positions, the elevation is assumed to be the level of the tide plus the influence of atmospheric pressure. Wave set-up was not included.

The main problem with rectifying the wet-dry boundary is that there is no a priori knowledge of the elevation of the pixels that mark the location of this boundary, since this boundary can be much higher than the shoreline (which is normally used for rectification). However, wet-dry pixels can be rectified by using surveyed information of the beach face topography. Unfortunately, full 2D surveys are rarely collected, and requiring such information to extract the wet-dry boundary would severely limit the usefulness of the technique (if such a survey was available, then it would be much easier to simply survey the wet-dry boundary rather than try to measure it from video). The main premise of using the video is to obtain high spatial and temporal coverage without labour-intensive and expensive field measurements. Rather than surveying the beach, it is also possible to use the tidal variations of the shoreline to map the intertidal topography (Aarninkhof et al., 2003; Plant and Holman, 1997). Normally, such a shoreline is extracted from the averaged images, and so a 2-D map of the interidal beachface is provided. However, due to the black sand characteristics of Ngaranui Beach, we have been unable to extract the shoreline from the averaged images using either published (e.g. Boak and Turner, 2005) or unpublished techniques. Therefore we could only extract the shoreline along the time stacks, where we could extract the shoreline using the variation of the swash as the tide moves up and down the beach face (described above). Therefore, we had 3 estimates

of the beach profile at each time-stack location, to use in rectifying the groundwater seepage line measurements along the 3 time-stack locations.

The profile information and the colinearity equations can be combined to perform the rectification in one computational step (e.g. Salmon et al., 2007; Bryan et al. 2008). For example if the profile can be described by function $f_1(z) = f_1(x,y)$, and the transformation associated with rectification described as $f_2(x,y)=f_2(u,v,z)$, where (u,v) are the oblique pixel coordinates and (x,y,z) the ground coordinates, then these two equations can be combined to find x and y without knowledge of z (or to find z from a known u and v). We approximated the profile using two linear fits, one for the upper beach face and one for the lower. These fits removed some of the variability caused by finding the shoreline using the average swash position, and also was used to average out the difference between the shoreline mapped using the incoming tide and that mapped using the outgoing tide. These fits were used to characterise the profile function (f_1), and provide 3 measurements of the elevation of the wet-dry boundary along each of the 3 timestacks.

3.2 Validation

Data from 3 field excursions was used to validate the methodology. On November 8th, 2010, an RTK-GPS survey was collected covering all three timestacks, allowing the method for extracting profiles from video to be validated on this beach. Madsen and Plant (2001) have validated the method in a general sense, but there may be local sensitivity in the method of extracting shorelines. On April 14, 2011, we made measurements of grain size, beach profile and sediment water content along two cross-shore transects (near timestacks 2 and 3) using an RTK-GPS. One transect was sampled at 10:20 am (near timestack 2) and the other transect was sampled at 12 pm (near timestack 3). In addition, sediment samples were taken at 5

11

minute intervals at 11:00, 11:05 and 10:10 (during the time which the camera was performing the averaging procedure) (near timestack 2). Sediment samples were collected using water-tight pots of known volume of the surface ~5 cm of sediments. Samples were weighed and then dried over 4 days at 80 degrees, and weighed again to determine water content. Grainsize was characterised using a Malvern Laser particle size analyser along one transect (near timestack 2) and at one site near the low-tide waterline (near timestack 3). After the measurements on April 14 indicated only minor differences in the sediment water content seaward and landward of the detected wet-dry boundary, another short experiment was undertaken on April 29th, 2011, to measure the elevation of the groundwater table relative to the beach face. A cross-shore transect of stilling wells (~tubes of 5 cm diameter with mesh at the lower end, buried to about 40cm deep) was deployed at 5 m spacing across the detected ground water seepage line (following the methodology in Bryan et al., 2009). The beach face and wells were surveyed using a Total Station into the same grid as the RTK-GPS measurements and the ground control points used to geo-reference the video camera. Water level in the wells relative to the top of the wells was measured using an electronic dip-well plumb (accuracy ~0.5 cm), and distance between the top of the wells and the beach face was measured using a measuring tape (accuracy ~0.5 cm). A rod was used to level the beach face around the wells prior to measurement. Four transects were measured, each at different stages of the falling tide, and different lighting conditions (due to changing cloud cover).

3.3 Data set selection

We selected fourteen days from the database of images for analysis during the period October 2007-July 2009, for which all (approximately twenty per day) half-an-hour time-averaged images and timestacks were analysed. The selection criteria were: 1) spring-tidal conditions, 2) high-quality images (i.e. no fog, heavy rain or sun glare), 3) ebb-tide occurring during

daylight hours and 4) a representative range of offshore wave conditions. Figure 5 shows the selected days together with all available wave, water level and rainfall data. Table 1 provides the wave, tide and rainfall conditions for the 14 selected days. The mean wave height during the whole period was $H_{sig,mean}$ = 1.85 m with a standard deviation of σ_H = 0.91 m. Days with $H_{sig} < H_{sig,mean} - 0.5\sigma_H$ are selected as low-wave events whereas high-wave events are days with $H_{sig} > H_{sig,mean} + 0.5\sigma_H$. Low-wave events ($H_{sig}$ < 1.39 m) occurred on day 3 and 12, which were during the Southern Hemisphere Summer (Table 1). A high-wave event (H_{sig} > 2.30 m) in summer occurred on day 1. In winter, low-wave events occurred on day 4, 7 and 14, high-wave events occurred on day 6, 8 and 13. On day 2, 5, 9, 10 and 11, wave heights were moderate (1.39 < H < 2.30 m). Excess rainfall (P > 75 mm) occurred the day prior to day 12 (Figure 5). A high cumulative rainfall, P_{cum} > 200 mm, occurred in the month (calculated over ~27 days) prior to day 8 and 14. Day 1, 2, 3, 4 and 5 were after a relatively dry month (P_{cum} < 60 mm, Table 1).

4 Results

4.1 Validation

The relationship (f_1) developed from the map of the intertidal region created using the variation of the shoreline and the tide compared well to the relationship derived using the surveyed beach profiles giving rms errors of 0.09 m, 0.07 m, 0.1 m for stack locations 1, 2 and 3 respectively (Figure 6). In each case the incoming tide mapped a profile that was below the true profile and the outgoing tide mapped a profile that was above the true profile and when a line was fit to the measurements, the result caused a bias that was slightly below. In addition to this error, we estimate a ~ 4 cm error originating from fitting the profile with two lines. This means that our method for evaluating the seepage face elevations resulted in elevations that were ~ 10±4 cm below the true seepage face values.

13

The results from the following two field experiments showed that the groundwater seepage line detected from video relates more to the level of the water table than to a distinct difference in the water content of sediments. The choice of threshold for the Value used to detect the seepage line corresponded to the water content of the sediment exceeding 42% (Figure 7, Panel F). Although this may depend on the cross-shore variation of grain size characteristics (Figure 7, Panel A), the results plotted on Figure 7A and F are from 3 different times, and two different locations (near timestacks 2 and 3), suggesting only minor sensitivity. The threshold of Value used to detect the wet-dry boundary corresponds to the point at which the groundwater table is less than 2±1 cm from the surface of the beach (Figure 7 B-E). Average grainsize near timestack 2 was 0.27 mm (medium sand), and the one sediment sample collected near timestack 3 was 0.43 mm.

3.2 Long term variations

Our analysis of the wet-dry boundary and shoreline elevations indicated 6 days where the difference in elevation between the wet-dry boundary and the shoreline, Δz, remained approximately constant as the tide varied (which we will define as 'coupled' ground water seepage line (GWSL)). During the other 8 days, the wet-dry boundary and the shoreline decoupled, and around low tide, the wet-dry boundary (which we will define as an 'uncoupled' GWSL) was at a much higher elevation than the shoreline. Figure 8 shows examples of both cases. In this Figure, the arrow shows that Δz at low tide is quite different in these two cases. In Figure 8B, the wet-dry boundary is super-elevated above the shoreline at low tide (coupled), whereas in Figure 8A, the Δz is not much different at low tide and at high tide (uncoupled). At high tide, Δz ranged between 0.1 and 0.8 m.

For days when a coupled GWSL developed (e.g. Figure 8A), we found Δz to depend

positively on run-up height, H_{ru}, and run-up period, T_{ru} (Figure 9, statistically significant at

the 95% confidence level). Here, H_{ru} was determined as the difference between the mean

minimum and mean maximum run-up from the timestacks. T_{ru} was determined for each

studied day from the mean time difference between the manually digitized maximum run-up

points in each individual timestack (Figure 3). Therefore on these days when a coupled

GWSL developed, the wet-dry boundary is likely related to the upper swash limit. This would

suggest that Δz was about equal to the difference in elevation of the run-up maxima and the

shoreline. From our analysis of the maximum run-up in relation to Δz on days without

decoupling, we found that Δz was about equal to the difference in elevation of the shoreline

and the 90% upper limit of the swash maxima. The increase in Δz with H_{ru} and T_{ru} reflects the

increasing importance of infragravity (0.004s−0.05s) waves to the swash, both through a

larger input of infra-gravity energy from offshore and through wave-wave overtaking in the

swash (Guza and Thornton, 1982; Ruessink et al., 1998). The wave-wave overtaking was

clearly visible from the timestacks, as not every individual incident wave resulted in a run-up

maximum. Outliers of Δz in Figure 9A and B may be caused by inadequacies in the

determination of the elevation of the wet-dry boundary due to, for instance, irregular beach

morphology. Here, the beach profile was approximated by two straight lines, one for the

upper beach face and one for the lower beach face, and the validation experiments indicate

that this could cause a minor error (~4 cm) in the calculation of Δz.

During 8 of the studied cases, the wet-dry boundary decoupled from the shoreline (e.g. Figure

8B), during ebbing tide. An uncoupled GWSL formed and Δz at low tide could exceed Δz at

high tide by up to 2 m. Considering all 8 days with decoupling of the GWSL and the

shoreline, the variance of Δz at high tide is 0.03 m^2 , which is considerably smaller than the

variance of Δz, 0.77 m^2, at low tide. This suggests that at low tide the variation in Δz is related to the elevation of the beach groundwater table, rather than to run-up parameters only. The photo in Figure 2 suggest that a decoupled seepage face might vary considerably spatially. Figure 10A shows a positive relation between Δz at low tide and the cumulative rainfall, P_{cum}, at all days (statistically significant at the 95% confidence interval). Figure 11 indicates that a summation period for P_{cum} between 12 and 40 days resulted in the highest correlations R^2 between P_{cum} and Δz at low tide. The lower R^2 for summation periods < 12 days suggests that an elevated low tide seepage line does not occur directly in response to a single large rain event. This might explain why the results for summer day 12 ($\Delta z \sim 0.3$ m, $P_{cum} \sim 150$ mm) appear to be anomalous in Figure 10A, because there was a single rain event 2 days prior to day 12 only. The cluster of points in Figure 10 A at $\Delta z \sim 2.5$ m and $P_{cum} \sim 230$ mm correspond to points that are anomalously high in the T_{ru} and Δz relationship shown in Figure 10B. When $P_{cum} < 200$ mm, T_{ru} and Δz at low tide are positively related (statistically significant at the 95% confidence level). This suggests that P_{cum} can be quite large (although still less than 200 mm), for the Δz at low tide to be somewhat influenced by run-up dynamics.

5 Discussion

The current findings show that video can be used to study the dynamics of the groundwater seepage line, as long as a method to deal with the vertical elevation needed for rectification is employed. Our results show that earlier techniques that based the detection of the shoreline on HSV (e.g. Aarninkhof et al., 2003) may only detect the shoreline in cases where the groundwater seepage line is close to the elevation of the shoreline. Otherwise, a HSV thresholding algorithm might detect the seepage line rather than the shoreline, which may be up to 2.5 m higher in elevation (corresponding in our case to ~ 150 m landward) than the true shoreline. Although, Ngaranui beach is a medium sand beach with unusually low slope, and

16

this low slope may account for the development of a seepage face, many other studies have shown the existence of a decoupled seepage face (e.g. Emery and Foster, 1948; Duncan, 1964; Nielsen, 1990; Turner et al., 1997). Other techniques, e.g. the SLIM algorithm (Madsen and Plant, 2001; Plant and Holman, 1997), define the shoreline based on the occurrence of a bright-band associated with shore break. This bright-band is, however, generally absent on dissipative beaches (Aarninkhof et al., 2003; Plant et al., 2007; Wright and Short, 1984). For example, the time-averaged image in Figure 4A does not show a bright-band for the swash zone at the current field site (the swash zone in Figure 4A is at the location of the white circles). Possibly, variance images can be used to track the shoreline, because at the shoreline run-up causes a continuous variation of high and low intensities leading to a high variance (Holland et al., 1999; Holman and Stanley, 2007; Pearre and Puleo, 2009), and attempts have been made to track shoreline using variance images; however, variance images were not collected in our study.

Our results show that the video detects two types of groundwater seepage line, one in which the shoreline and seepage line are decoupled and one in which they are coupled and so the seepage line is influenced by swash. When the groundwater seepage line was within the range of run-up (coupled), depending on the run-up amplitude, there was a probability that the run-up would overtop the seepage line, and cause a local increase in the seepage line. In the second case, the groundwater seepage line was higher than the range of maximum run-up, and so was unaffected by ground water variations. When the seepage line was coupled with the shoreline, examination of the timestacks showed that the seepage line increased in elevation each time an anomalously high swash event overtopped the seepage line. When the shoreline and GWSL were strongly coupled, this occurred regularly, and as the GWSL and shoreline decouple, the probability of this occurring gradually decreases. Figure 9 shows that the

17

influence of swash height and period become increasing less important as the degree of coupling increases. The steepness of the cross-shore profile in Value (Figure 4B) near the seepage line depends on the rate of change of the seepage line during the 10 minute stack period, which in turn will depend on (1) the swash variations when Δz is small and (2) the low tide Δz value when the seepage line and shoreline are decoupled. The low tide Δz value and the tidal range will determine the elevation change of the seepage line between high and low tide (and the speed at which the seepage line moves across the beachface). The timestack displayed in Figure 3 shows a slowly falling seepage line, unaffected by the swash variations.

Our technique for measuring the groundwater seepage line from video has a number of errors which we estimate to be smaller than the Δz measurements we made in the majority of cases. The validation experiments suggest that the largest source of error is caused by determining the beach profile using the shoreline variation across the beach face over a tidal cycle. Figure 6 shows that although the shorelines detected on the incoming and outgoing tide were lower and higher than the actual waterline, fitting a profile line caused an error in elevation of order 10 cm ± 4cm. The bias in our shorelines may be caused by neglecting the effect of wave set-up (Aarninkhof et al., 2003 include this). The bias may be caused by the relationship between the mean waterline as detected by an array of stilling wells and the water line detected by the averaging swash variations. Bryan et al. (2008) use measurements from an intermediate medium sand beach to show that there may be differences of order 1.5m in the horizontal and, considering their beach slope of 0.025, ~ 0.04 m in the vertical. Presumably these differences would depend on the statistical characteristics of swash which are influenced by wave height and period, beach slope (Huntley et al., 1977), tidal variations (Guedes et al., 2011) and friction (e.g., Raubenheimer et al., 2004), and could be larger on a dissipative beach. Finally our thresholds for detecting seepage line from the Value measurements provide measurements

18

that are within a few centimetres of the elevation of true groundwater seepage line (as measured by stilling wells). It is possible that variations to the optical characteristics of the sand will also change these thresholds. Therefore, although our method is universally-applicable, and the patterns we detect are greater than the possible sources of error, validation of both the intertidal mapping algorithms and the thresholds used in image processing should be undertaken for research applications at new field sites.

The present results indicate that there is a positive relation between the P_{cum} of 15-30 days prior to the analysed days and Δz at low tide (Figure 11). The increase of groundwater level with rainfall is consistent with Horn (2002), Horn (2006) and Turner et al. (1997), who stated that rainfall increases the elevation of the beach water table and causes therefore a super-elevation of the GWSL above the shoreline. Turner et al. (1997) related the elevation of the GWSL to the significant rainfall over 48 hours (>200 mm), however, they did not analyse the relation to P_{cum} over a longer summation period and this type of results are likely to be driven by the local setting. Our data do not show a direct relationship between the elevation of the GWSL and the rainfall occurring on the day of sampling. This might be due to the difference in morphology of the beach between the present research and the research of Turner et al. (1997). The correlation with P_{cum} was relatively low, either indicating that P_{cum} was not linearly related to the water table elevation, which is not surprising given the complex dynamics of water movement through coastal aquifers. We also did not find a correlation with the spring tidal range, and correlations with H_{ru} and T_{ru} occurred only when Δz was small. A shortcoming of this work is that we did not measure the temporal variation of grainsize characteristics even though the measurements taken during the validation experiments are similar to 0.31 mm reported in Laurent (2000). Simple calculations using the SEEP model provided in Turner (1993) indicate that grain size variations of 0.23 m – 0.43 m (the extremes

19

that we measured) would only cause variations to the seepage face height of < 1cm, so it is safe to assume that variations in the hydraulic conductivity would not explain the changes to Δz that we observed.

In summary, our results (14 cases) show that when there has been a high level of rainfall during the previous month (~57% of the cases) the water table becomes elevated relative to the mean sea level. In this case the water does not seep rapidly enough through the beach face for the seepage line to fall with the tide. We speculate that this is not because the hydraulic conductivity of the beach changes between these events, but because there is a higher pressure gradient on the beach caused by the elevation difference between mean sea level and the water table. In the remaining 43% of cases, the inland water table was likely to be much lower, so the horizontal pressure gradient was smaller, and the hydraulic conductivity sufficiently high relative to the pressure gradient for the water to drain from the beach face at a similar rate than the falling tide. In these cases, swash can occasionally overtop the seepage line and cause small increases to the seepage line. The probability of this occurring is greater with larger swash periods and heights. Having only sampled 14 cases, with the main objective to test whether it is useful to develop a technique to extract decoupled seepage line variations from video, we do not know whether our results represent the natural variation of the seepage line characteristics at Ngaranui Beach. The influence of rainfall on beach groundwater dynamics is often not taken into account in existing models. Our study suggests that besides run-up characteristics, cumulative rainfall may partly cause the super-elevation of the beach water table, and we thus cannot ignore the latter process in modelling groundwater seepage.

6 Conclusions

The dynamics of the seepage line and the shoreline have been investigated using video-imagery. A useful method to extract the wet-dry boundary in video imagery is proposed, using variations in Value in oblique video images which are rectified using the beach profile generated as the videoed shoreline moves across the beachface. The method was tested against validation data, and estimates of error are on the order of 0.15 m. This methodology is necessary when the seepage line is decoupled from the shoreline, so that the sealevel cannot be used for rectification. This occurred often (~50%) in the cases tested on this medium-sand, low-sloped beach. The method is expected to be applicable on beaches characterized by low slopes, fine grain sizes and large tidal ranges, and will be evident when the separation between the swash zone (as detected in timestacks or variance images) and the region of rapidly changing Value in the time-averaged images is greater at low tide than at high tide.

When the seepage line is coupled with the shoreline, the seepage line variations during the tidal cycle are related to swash dynamics. When the groundwater seepage line decouples from the shoreline with falling tide, the super-elevation of the GWSL above the shoreline at low tide is related to the cumulative rainfall in the preceding 15−30 days and to a lesser extent to the swash variations. The super-elevation is not related to incidental rainfall, but only to a high cumulative rainfall. At high tide, the groundwater seepage line was always coupled to the shoreline and varied with the influence of swash dynamics only.

The outcomes of this study encourage further use of video imagery to investigate the changes in groundwater seepage characteristics over large spatial and temporal scales and the influence of these on beachface erosion and accretion patterns. Earlier techniques that identify the shoreline as the wet-dry boundary in Hue-Saturation-Value space will only be valid when

21

coupling occurs, otherwise, they will identify the groundwater seepage line and not the shoreline.

References

Aagaard, T., Holm, J., 1989. Digitization of wave run-up using video records. Journal of Coastal Research 5(3), 547–551.

Aarninkhof, S. G. J., Turner, I. L., Dronkers, T. D. T., Caljouw, M., Nipius, L., 2003. A video-based technique for mapping intertidal beach bathymetry. Coastal Engineering 49 (4), 275–289.

Almar, R., Coco, G., Bryan, K. R., Huntley, D. A., Short, A. D., Senechal, N., 2008. Video observations of beach cusp morphodynamics. Marine Geology 254 (3-4), 216–223.

Baird, A. J., Horn, D. P., 1996. Monitoring and modelling groundwater behaviour in sandy beaches. Journal of Coastal Research 12 (3), 630–640.

Baird, A. J., Mason, T., Horn, D. P., 1998. Validation of a boussinesq model of beach ground water behaviour. Marine Geology 148 (1), 55–69.

Boak, E. H., Turner, I.L., 2005. Shoreline Definition and Detection: A Review. Journal of Coastal Research 21 (4) pp. 688 – 703.

22

Bryan K. R., Summer, S. A., Coco, G., 2008. Measuring storm run-up on beaches using video, 31st International Conference on Coastal Engineering, AUG 31-SEP 05, 2008 Hamburg, Germany, 854-946.

Butt, T., Russell, P., Turner, I., 2001. The influence of swash infiltration-exfiltration on beach face sediment transport: Onshore or offshore? Coastal Engineering 42 (1), 35–52.

Cartwright, N., Baldock, T. E., Nielsen, P., Jeng, D., Tao, L., 2006. Swash-aquifer interaction in the vicinity of the water table exit point on a sandy beach. Journal of Geophysical Research 111 (C9), 9035.

Coco, G., Werner, B.T., Burnet, T., Elgar, S., 2004. The role of tides in beach cusp formation, Journal of Geophysical Research, 109, CO4011, doi: 10.1029/2003JC002154.

Duncan, J. R., 1964. The effects of watertable and tide cycle on swashbackwash sediment distribution and beach profile development, Marine Geology, 2, 186–197.

Eliot, I. G., Clarke, D. J., 1988. Semi-diurnal variation in beachface aggradation and degradation. Marine Geology 79 (1-2), 1–22.

Emery, K. O., and J. F. Foster, 1948. Watertables in marine beaches, Journal of Marine Research, 7, 644–654.

Gallop, S. L., Bryan, K.R., Coco, G., 2011. Storm-driven changes in rip channel patterns on an embayed beach, Geomorphology 127 (3-4), 179-188.

Gorman, R. M., Bryan, K. R., Laing, A. K., 2003. Wave hindcast for the new zealand region: nearshore validation and coastal wave climate. New Zealand Journal of Marine and Freshwater Research 37 (3), 567–588.

Grant, U. S., 1948. Influence of the water table on beach aggradation and degradation. Journal of Marine Research 7 (3), 655–660.

Guedes, R. M.C., Bryan, K. R., Coco, G., Holman, R. A., 2011. The effects of tides on swash statistics on an intermediate beach, Journal of Geophysical Research 116, C04008, dio: 10.1029/2010JC006660.

Guza, R. T., Thornton, E. B., 1982. Swash oscillations on a natural beach. Journal of Geophysical Research 87 (C), 483–492.

Heikkilä, J., Silven, O., 1997. A four-step camera calibration procedure with implicit image correction. In: Proceedings of the 1997 Conference on Computer Vision and Pattern Recognition (CVPR'97). IEEE Computer Society Washington, DC, USA.

Holland, K.T., and Holman, R.A., 1993. The statistical distribution of swash maxima, Journal of Geophysical Research, 98, C6, 10271-10278.

Holland, K. T., Vincent, C. L., Holman, R. A., 1999. Statistical characterization of nearshore morphodynamic behavior. In: Proceedings Coastal Sediments. Vol. 99. pp. 2176–2189.

Holman, R. A., Stanley, J., 2007. The history and technical capabilities of argus. Coastal Engineering 54 (6-7), 477–491.

Horn, D. P., 2002. Beach groundwater dynamics. Geomorphology 48 (1-3), 121–146.

Horn, D. P., 2006. Measurements and modelling of beach groundwater flow in the swash-zone: a review. Continental Shelf Research 26 (5), 622–652.

Huntley, D. A., Guza, R. T., Bowen, A. J., 1977. A universal form for the shoreline run-up spectra? Journal of Geophysical Research 82(18), 2577-2581. doi: 10.1029/JC082i018p02577.

Jackson, N. L., Horn, D. P., Spalding, V., Nordstrom, K. F., 1999. Changes in beach water table elevation during neap and spring tides on a sandy estuarine beach, delaware bay, new jersey. Estuaries and Coasts 22 (3), 753–762.

Komar, P. D., 1998. Beach processes and sedimentation. Vol. 2nd ed. Upper Saddle River, NJ Prentice Hall.

Laurent, J. C., 2000. The provenance and dispersal of beach sands on the west coast of the north island, new zealand. Master's thesis, Earth Sciences, University of Waikato, Hamilton, New Zealand.

Li, L., Barry, D. A., 2000. Wave-induced beach groundwater flow. Advances in Water Resources 23 (4), 325–337.

Li, L., Barry, D. A., Pattiaratchi, C. B., Masselink, G., 2002. Beachwin: modelling groundwater effects on swash sediment transport and beach profile changes. Environmental Modelling & Software 17 (3), 313–320.

Li, L., Barry, D. A., Stagnitti, F., Parlange, J. Y., Jeng, D. S., 2000. Beach water table fluctuations due to spring-neap tides: moving boundary effects. Advances in Water Resources 23 (8), 817–824.

Madsen, A. J., Plant, N. G., 2001. Intertidal beach slope predictions compared to field data. Marine Geology 173 (1-4), 121–139.

Morris, B. D., Coco, G., Bryan, K. R., Turner, I. L., 2007. Video-derived mapping of estuarine evolution. Journal of Coastal Research, SI 50, 410–414.

Nielsen, P., 1990. Tidal dynamics of the water table in beaches. Water Resources Research 26 (9), 2127–2134.

Pearre, N. S., Puleo, J. A., 2009. Quantifying seasonal shoreline variability at rehoboth beach, delaware, using automated imaging techniques. Journal of Coastal Research 25 (4), 900–914.

Plant, N. G., Aarninkhof, S. G. J., Turner, I. L., Kingston, K. S., 2007. The performance of shoreline detection models applied to video imagery. Journal of Coastal Research 23 (3), 658–670.

Plant, N. G., Holman, R. A., 1997. Intertidal beach profile estimation using video images. Marine Geology 140 (1-2), 1–24.

Raubenheimer, B., Elgar, S., Guza, R. T., 2004. Observations of swash zone velocities : a note on friction coefficients. Journal of Geophysical Research 109, C01027, doi:10.1029/2003JC001877.

Raubenheimer, B., Guza, R. T., Elgar, S., 1999. Tidal water table fluctuations in a sandy beaches. Water Resources Research 35, 2313–2320.

Ruessink, B. G., Kleinhans, M. G., Van den Beukel, P. G. L., 1998. Observations of swash under highly dissipative conditions. Journal of Geophysical Research 103 (C2), 3111–3118.

Russ, J. C., 2006. The image processing handbook, 5th Edition. CRC press, Boca Raton, Florida, USA.

Salmon, S. A., Bryan, K. R., Coco, G., 2007. The use of video systems to measure run-up on beaches. Journal of Coastal Research SI 50, 211–215.

Smith, A.R., 1978. Color Gamit Transform Pairs. SIGGRAPH 78, Conference Proceedings, Aug 1978, 12-19.

Stockdon, H. F., Holman, R. A., Howd, P. A., Sallenger Jr., A. H., 2006. Empirical parameterization of setup, swash, and runup. Coastal Engineering 53 (7), 573–588.

Turner, I. L., 1993. Water table outcropping on macro-tidal beaches: A simulation model. Marine Geology 115 (3), 227–238.

Turner, I. L., 1995. Simulating the influence of groundwater seepage on sediment transported by the sweep of the swash zone across macro-tidal beaches. Marine geology 125 (1-2), 153–174.

Turner, I. L., Coates, B. P., Acworth, R. I., 1997. Tides, waves and the super-elevation of groundwater at the coast. Journal of Coastal Research 13 (1), 46–60.

Turner, I. L., Leatherman, S. P., 1997. Beach dewatering as a 'soft' engineering solution to coastal erosion - a history and critical review. Journal of Coastal Research 13 (4), 1050–1063.

Walters, R. A., Goring, D. G., Bell, R. G., 2001. Ocean tides around new zealand. New Zealand Journal of Marine and Freshwater Research 35 (3), 567–580.

Wood, A., 2010. Episodic, seasonal, and long term morphological changes of Coromandel beaches, Unpublished MSc Thesis, University of Waikato.

Wright, L. D., Short, A. D., 1984. Morphodynamic variability of surf zones and beaches: a synthesis. Marine Geology 56 (1-4), 93–118.

FIGURES

Figure 1: A map of Ngaranui Beach, Raglan, New Zealand.

Figure 2: A snap-shot photo of swash and the groundwater seepage face at Ngaranui Beach, Raglan, New Zealand. (photo provided by Dave Roper). Groundwater seepage occupies the upper part of the beach and can be seen because of its shiny appearance. The swash zone is offshore of the seepage face. Channels draining the beachface can be seen in the upper part of the beach.

Figure 3: Example of a timestack. The white curved features in the image represent breaking waves and bores propagating onshore with time, ending as swash and backwash (run-up oscillations) on the beach. The maximum run-up points are marked with black circles (the mean is the bold white line on the right side), the minimum run-up points are marked with black stars (the mean is the leftmost white bold white line). Maximum and minima are digitized manually. The run-down minimum is at the intersection of the run-down (which is outward-moving intensity minimum in the image) with the following run-up. The mean run-up, swash mean, or shoreline is the black bold line. The grey featureless area to the right of the run-up oscillations is the subaerial saturated beach, and the brown area to the far right of the image is the unsaturated beach.

Figure 4: A) Example of a time-averaged image. The thick white alongshore line is the detected wet-dry boundary. The open white circles are position of the shoreline along the cross-shore lines of the individual timestacks. The locations of the timestacks are plotted with a long-dashed white lines. The crosses are the positions of the bench marks used for surveying (and also used for the beach profiles done in Wood (2009), which are marked with short-dashed white lines). B) An example of the Value from the time-averaged image along the second timestack position. The dashed line is the rawdata, and the bold grey line is the Value smoothed with a 10-pixel moving average. The threshold used for detecting the wet-dry boundary is marked with a horizontal black line and the intersection of the Value and the threshold is marked with a black cross.

Figure 5: Tidal water level fluctuation (A), wave height (B), wave period (C) and daily precipitation (D) at Ngaranui Beach. Vertical lines are the days selected for analysis.

Figure 6: The beach profile along the 3 time stacks (stack 1: diamonds, stack 2: squares, stack 3: circles). The open symbols are the profiles extracted from video and the filled symbols are the surveyed beach profiles. The dashed lines are the best fit lines to the surveyed profiles, and the solid lines are the best fit lines to the video-derived profiles. Data were collected on the 7th (video) and 8th (survey) of November, 2010.

Figure 7: Panel A: Sediment characteristics at the approximate location of timestack 2 collected on April 14th, 2011. Panels B-E, the cross-shore distribution of Value (thin lines, right hand scale) extracted from the image at the approximate location of timestack 2, taken on April 29th, 2011. The water table elevation relative to the beach face (thick lines, left hand scale). Vertical dotted lines correspond to the Value threshold used for that image. Panel F: Cross-shore distribution of sediment water content taken at 2 different locations on April 14th, 2011, close to the positions of timestacks 2 and 3 (lines, left scale). The Value data have been normalised and standardised. Cross-shore distribution of water content (circles, left scale).

Figure 8: Examples of the elevation of the shoreline (black circles) and of the seepage line (white triangles) over a tidal cycle. In case A) the separation of the groundwater seepage and

shoreline is the similar at low and high tide and B) the groundwater seepage line and shoreline separation is much larger at low tide than high tide.

Figure 9: The elevation difference, Δz, versus a) run-up period, T_{ru} and b) run-up height, H_{ru}, for the days with a coupled seepage line. The vertical lines represent the distribution of Δz at increasing classes of H_{ru} and T_{ru}. The circles represent the median in each class, and the bar represents the 90% and 10% ranges in each class.

Figure 10: The elevation difference Δz between the shoreline and the seepage line for all days at low tide, $Δz_{LT}$, versus a) the cumulative rainfall prior to the analysed day, P_{cum},(calculated over 27 days) and b) the period of the wave run-up at the beach, T_{ru}. Black (gray) dots refer to winter (summer). The cumulative period for P_{cum} is taken as 27 days (highest R^2 in Figure 11). However, the results were essentially the same for all P_{cum} in the range between 12 and 40 days. Each day is represented by 3 dots, one for each timestack. The dots with Δz at low tide >~ 0.8 m correspond to situations when a GWSL developed.

Figure 11: Goodness-of-fit, R^2, of the correlation between Δz and P_{cum}, where the range over which P_{cum} is calculated is varied from 1 to 70 days.

TABLES:
Table 1: Conditions during the 14 days chosen for analysis, where H_{sig} is the significant wave height, T_{mean} is the mean spectral period, P is the rainfall on the day of sampling, and P_{cum} is the cumulative rainfall.

27

Day	Date	H_{sig} (m)	T_{mean} (s)	Tidal Range (m)	P (mm)	P_{cum}[1] (mm)
1	26/10/2007	2.88	7.61	3.43	0	59.9
2	8/11/2007	1.63	5.75	2.32	0	56.2
3	9/12/2007	0.77	8.39	2.5	0	43.5
4	21/03/2008	1.06	8.29	2.85	0	31.1
5	5/04/2008	1.69	9.35	3.14	0	55
6	19/04/2008	2.81	7.36	2.52	0	110.5
7	19/05/2008	0.87	6.62	2.44	0	143.9
8	1/08/2008	3.14	6.81	3.08	14.4	229.5
9	15/09/2008	1.46	7.98	2.98	0	107.8
10	26/11/2008	1.71	8.18	2.29	0	69.5
11	12/12/2008	1.65	5.78	3.01	0	69.9
12	26/12/2008	1.06	7.43	2.06	0	151.7
13	10/03/2009	2.30	6.71	3.06	0	151.3
14	24/05/2009	1.36	7.59	3.02	2	204.4

[1]Cumulative rainfall over the preceding 27 days

Table 1:

28

Rangipu

South
Head (81 m)

Ngarunui Beach

Tasman Sea

Manu Bay

CamEra Raglan B

0 250 500 1.000 1.500 2.000
Meters

N

1:750.000

1:30.000.000

N

N

Figure2

Figure3

Figure4

Figure5

A z_{tide} [m]

B H_{sig} [m]

C T_{mean} [s]

D P [mm]

time [mm/yy]
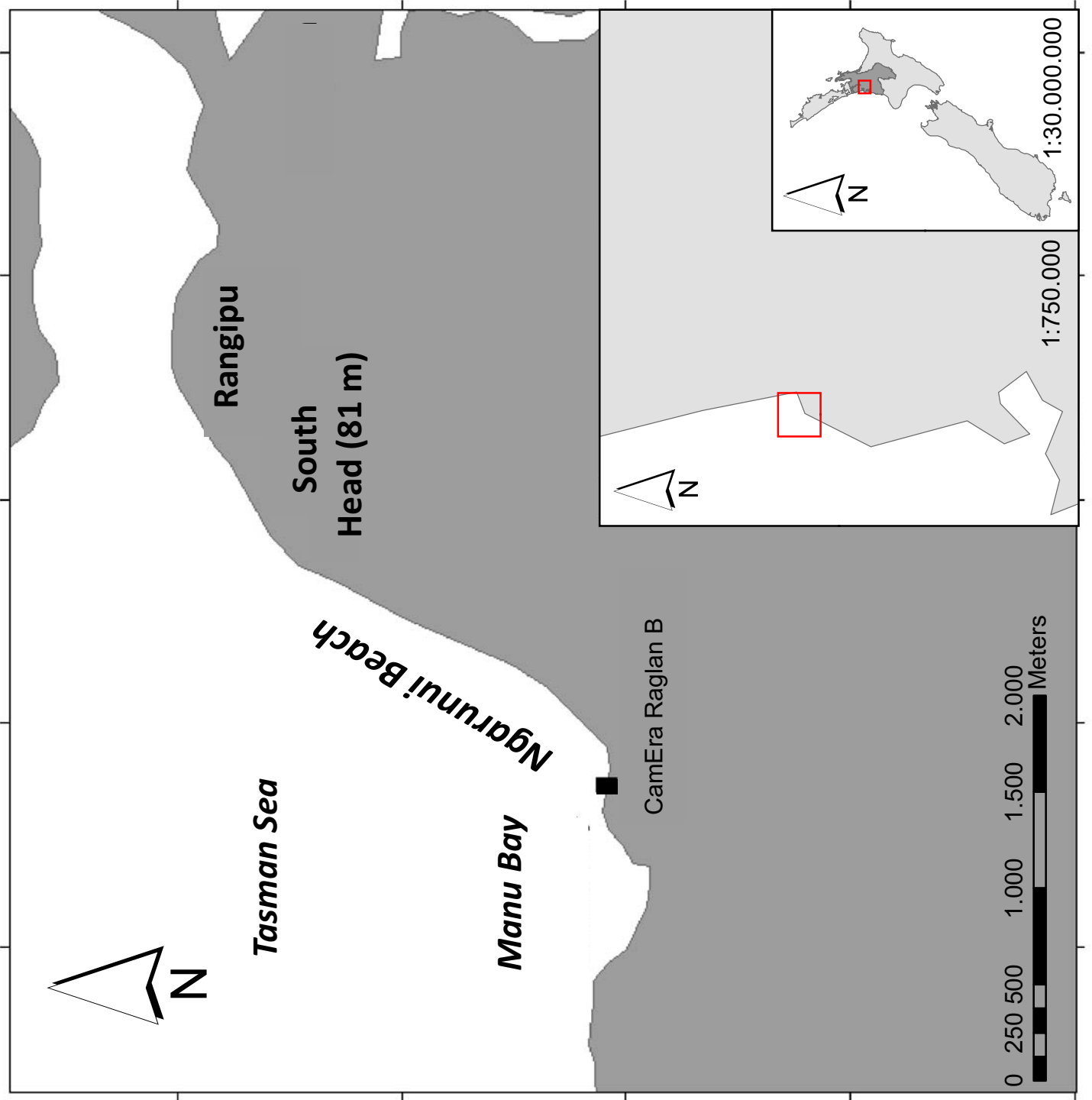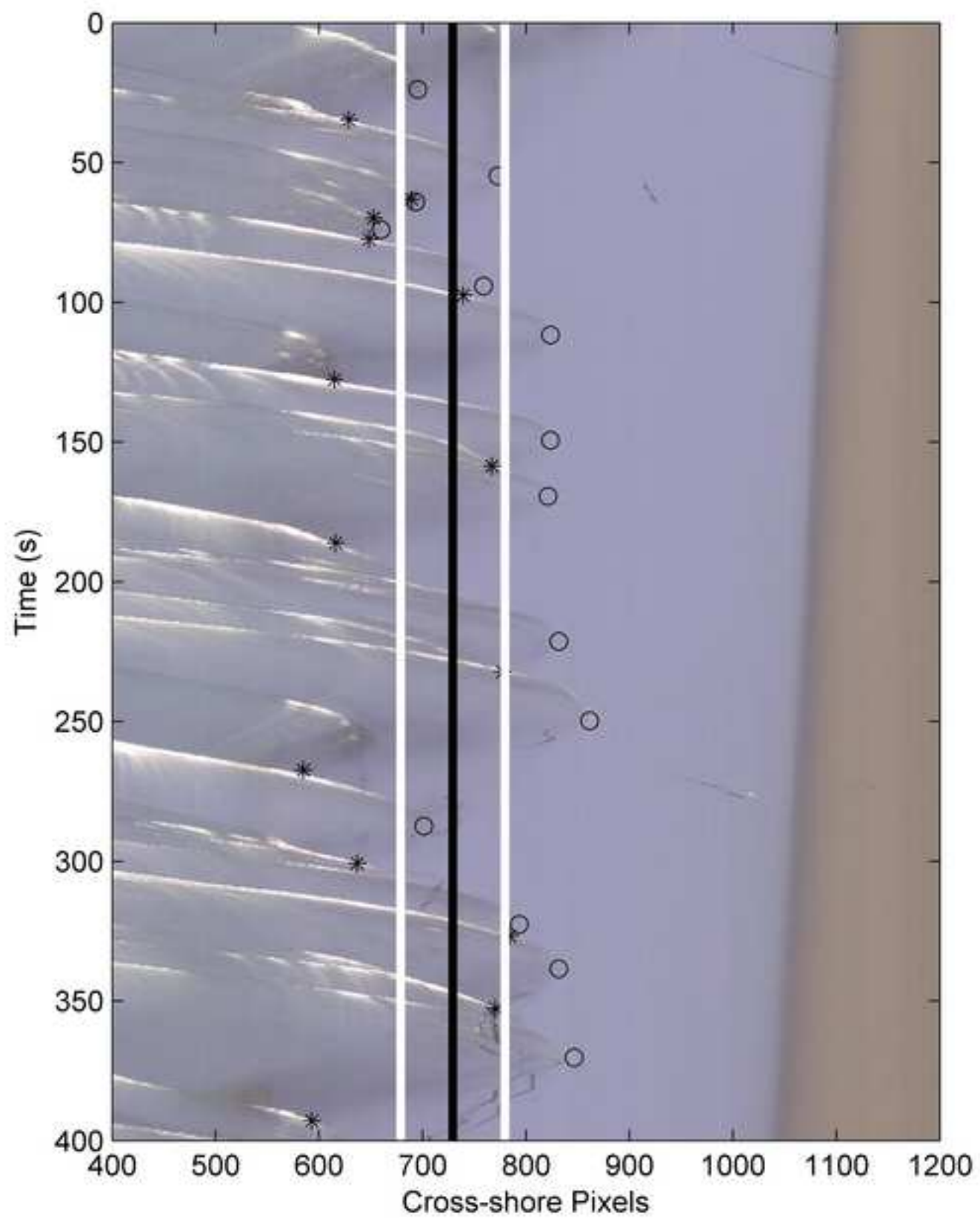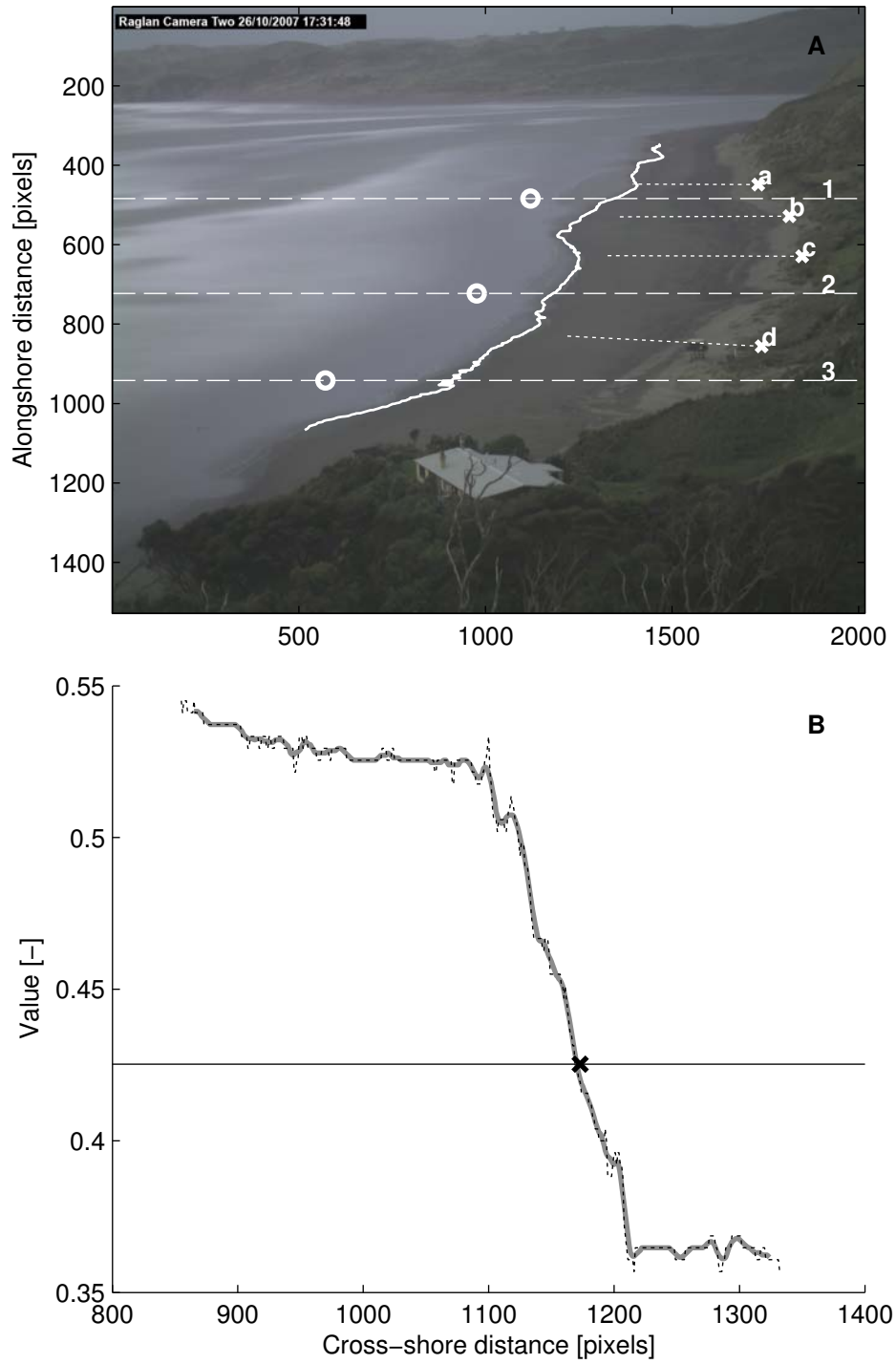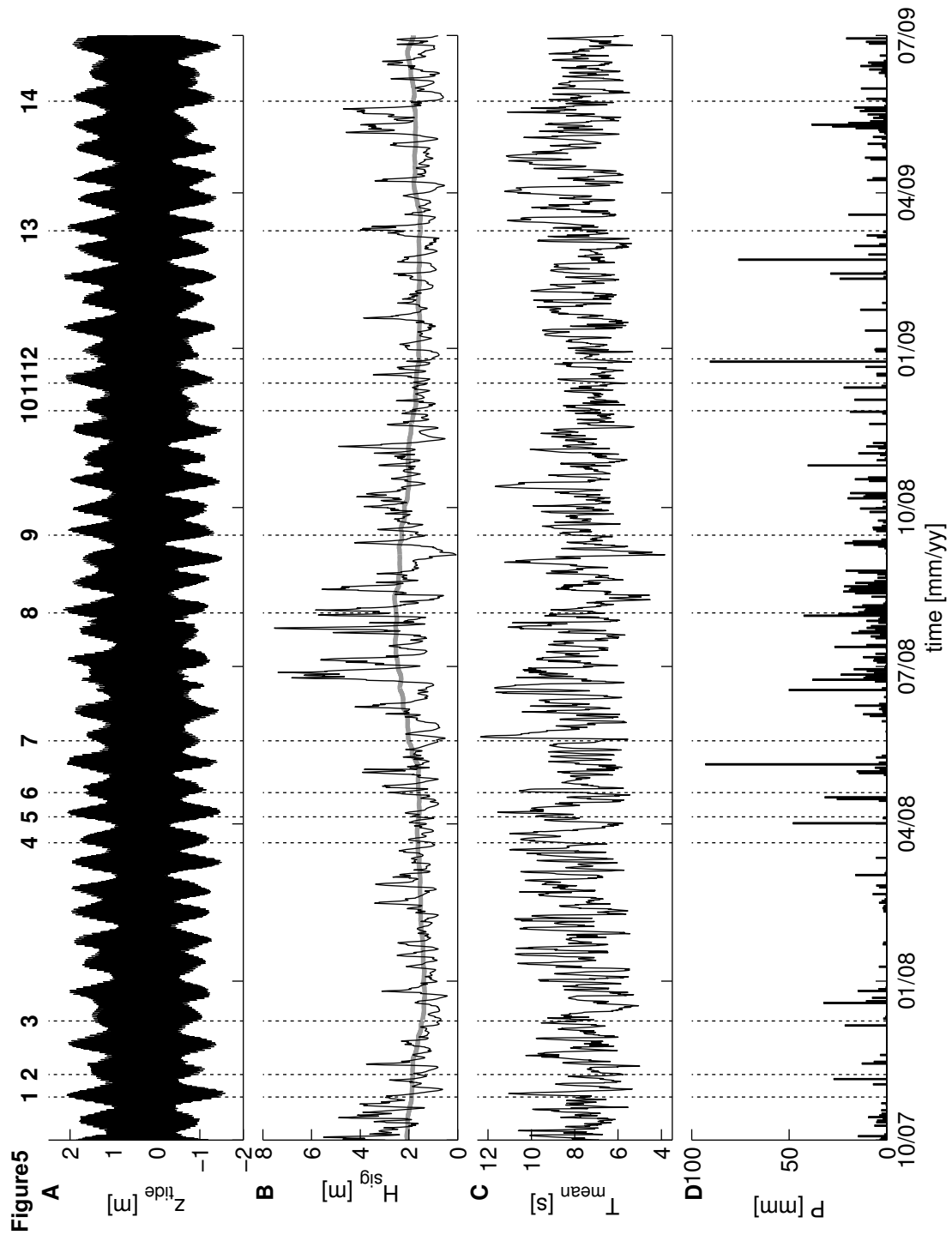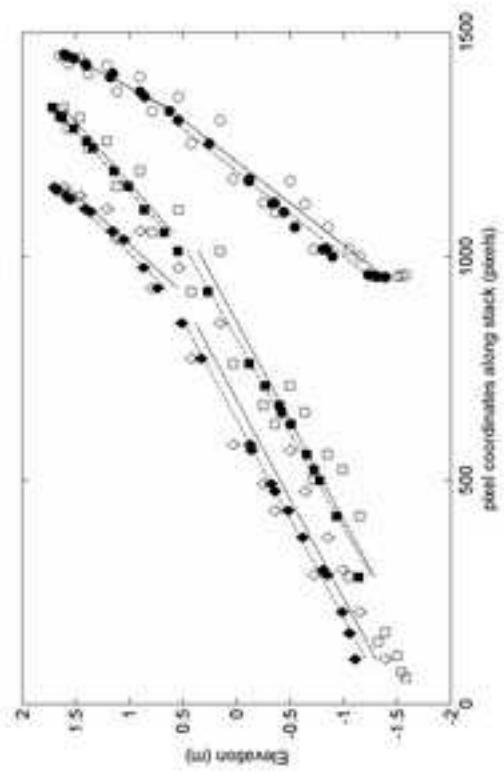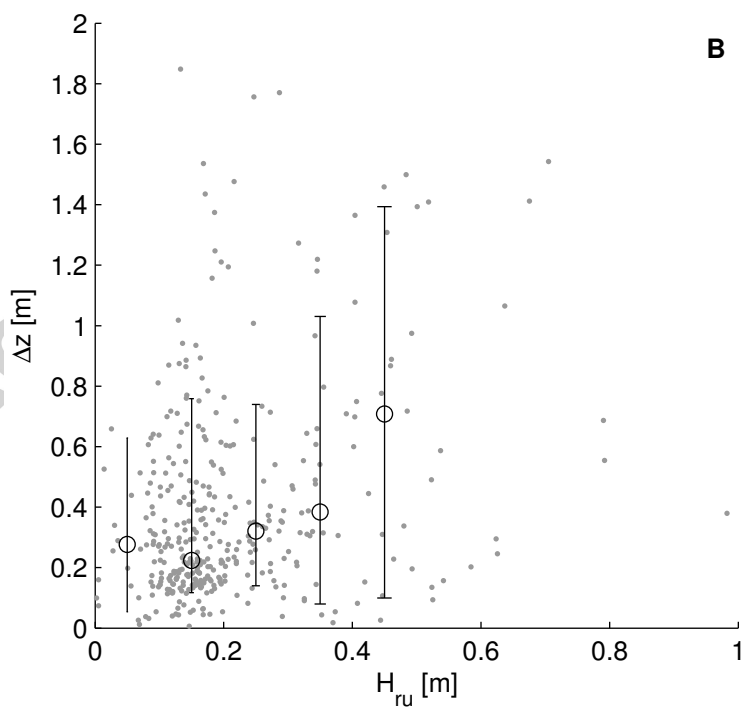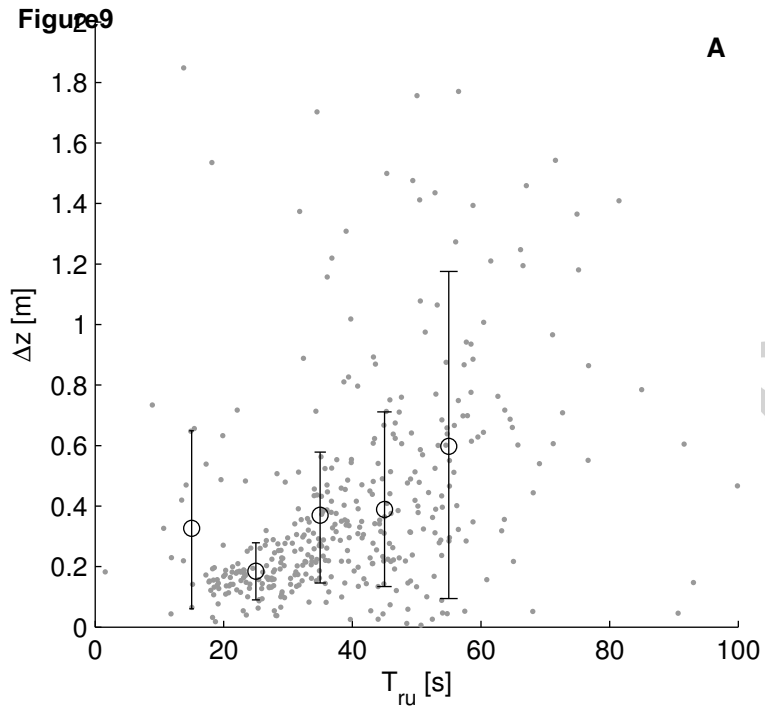
Figure6
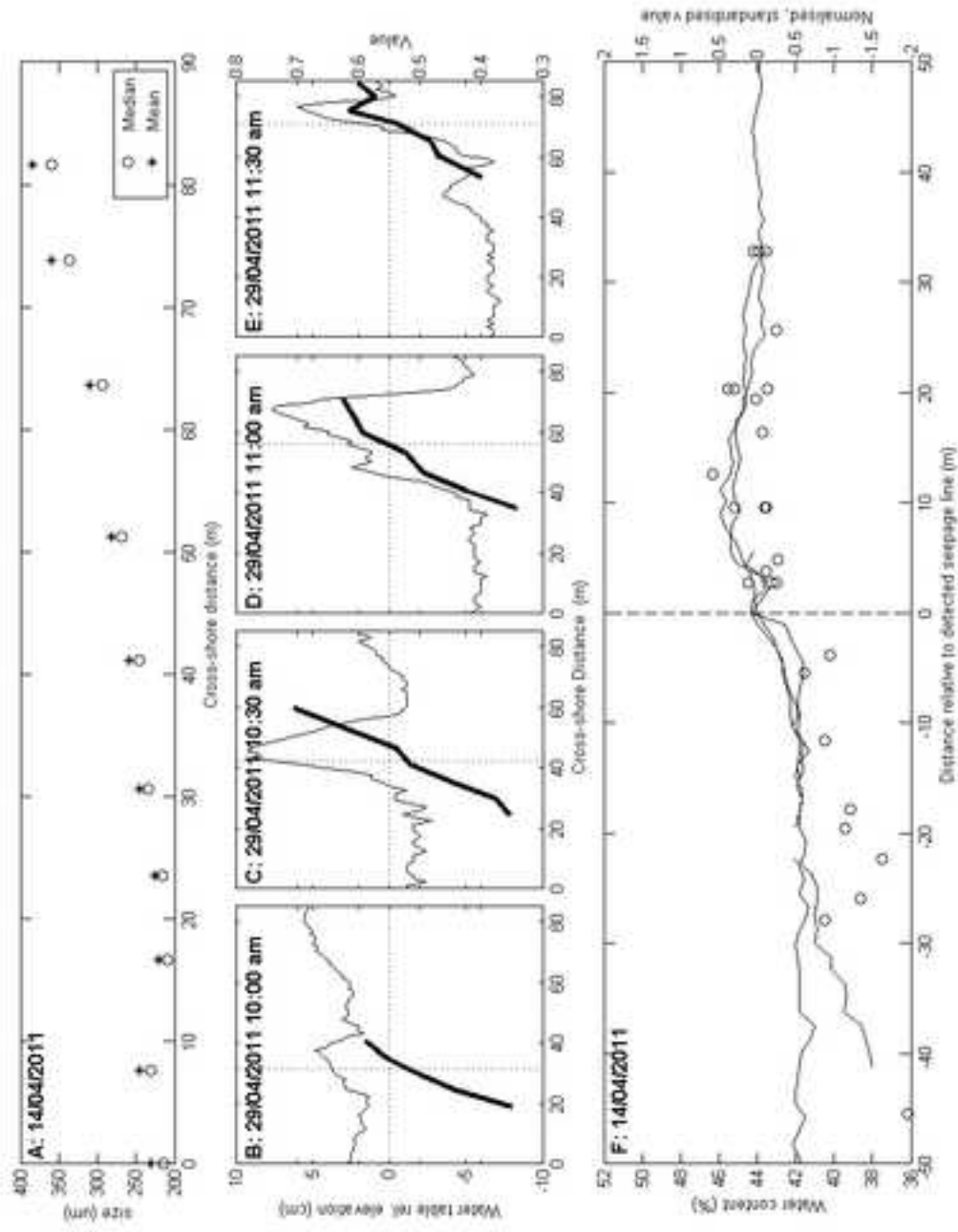
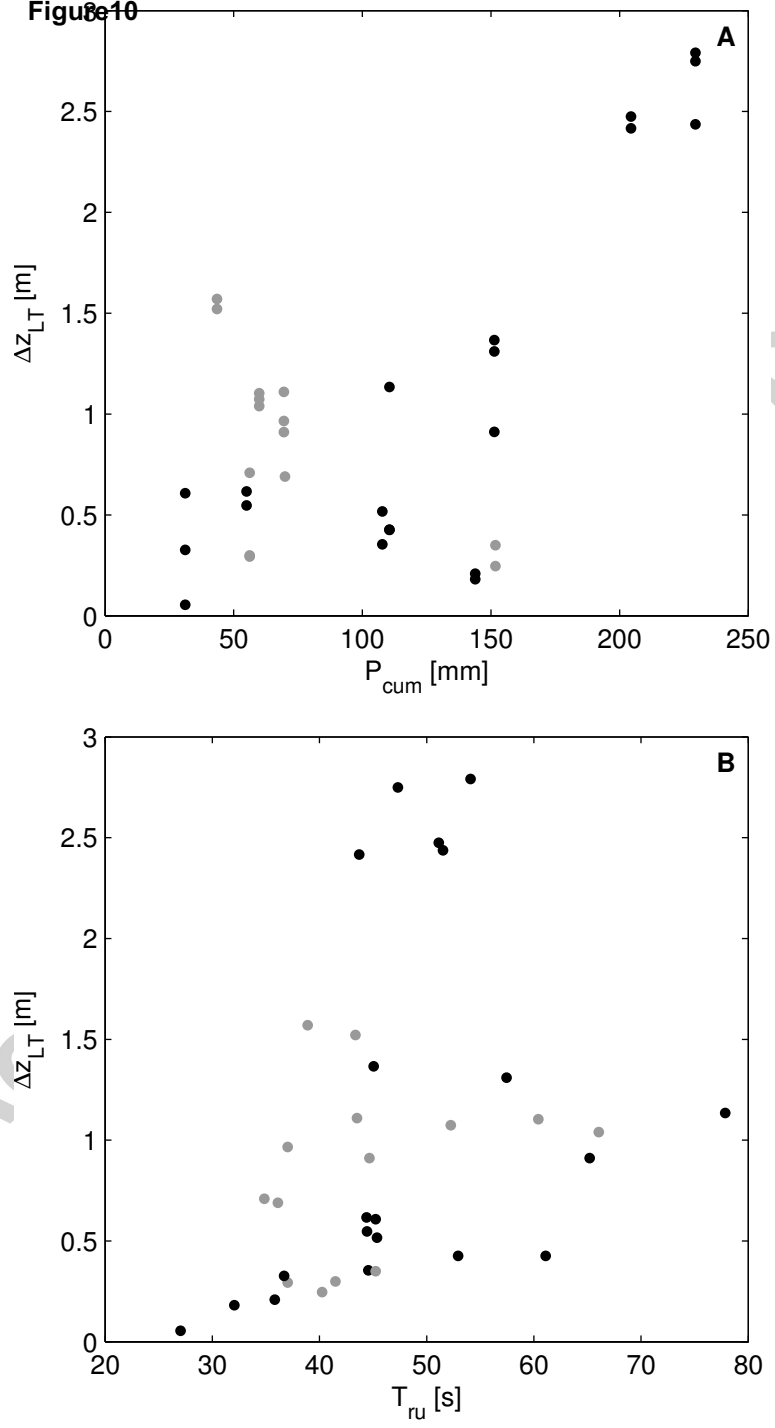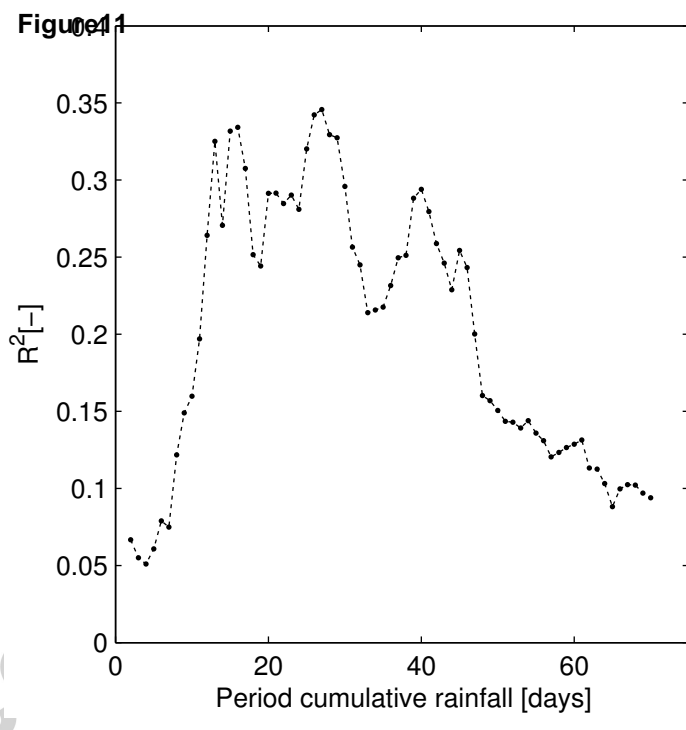**Figure7**
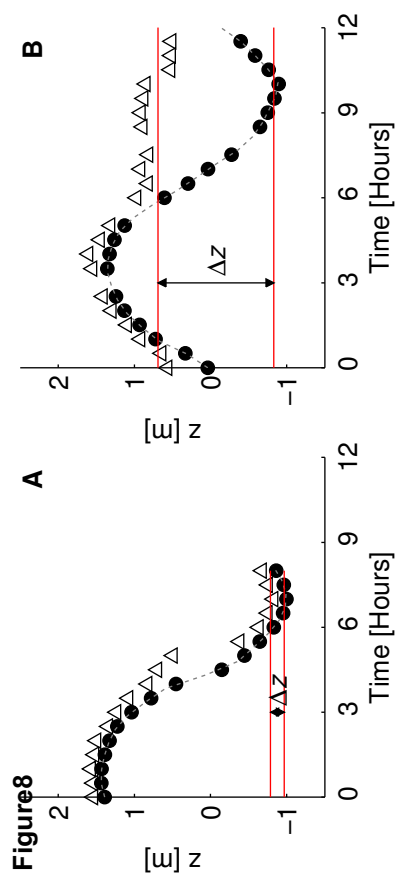
Figure8

Figure 9

Figure 10

Figure 11

Research highlights
- New method proposed to extract the wet-dry boundary in video imagery using the Value.
- Wet-dry boundary is related to groundwater seepage on specific kind of sand beaches.
- Wet-dry boundary may not always be a good indicator of the position of the shoreline.